Research Article | Vol. 9, No. 11 / 1 November 2019 / Optical Materials Express 4301
Optical Materials EXPRESS

Ge-capped SiGe core optical fibers

Wei Wu,[1] Mustafa H. Balci,[1] Korbinian Mühlberger,[2] Michael Fokine,[2] Fredrik Laurell,[2] Thomas Hawkins,[3] John Ballato,[3] and Ursula J. Gibson[1,2,*]

[1]Department of Physics, Norwegian University of Science and Technology, N-7491 Trondheim, Norway
[2]Department of Applied Physics, KTH Royal Institute of Technology, Stockholm 10044, Sweden
[3]Department of Materials Science and Engineering, Clemson University, Clemson, SC 29634, USA
*ursula.gibson@ntnu.no

Abstract: CO_2 laser processing offers the possibility to inscribe structures within glass-clad SiGe-core fibers by altering the spatial distribution of the Si and Ge. Spatial segregation of Ge to the end of a fiber is shown via optical transmission measurements used to alter the local bandgap, and the curved end of the fiber focuses the output of a multimode fiber. Scalable fabrication is demonstrated using a commercial CO_2 laser engraver for processing of arrays.

1. Introduction

Semiconductor-core optical fibers are of interest due to their optoelectronic properties [1], large non-linear coefficients [2] and the infrared (IR) transparency [3] associated with the core materials. Non-linear effects have been demonstrated with elemental silicon cores [2,4,5], and both laser processing [6] and fiber tapering [7] have been shown to improve fiber properties. SiGe alloys have been explored as cores to make IR transmitting fibers [8], and modification of the local composition of those fibers using lasers has been demonstrated both for the formation of grating structures [8] and for the fabrication of microparticles with segregated composition [9] in the core. The ability to structure the core has potential applications including detector arrays and solar cell fabrication. Local compositional variation potentially enables the fabrication of in-fiber diodes, as anticipated by Gumennik, et al. [10]. In this paper, we demonstrate axial structuring of SiGe core fibers and resultant optical effects, using a commercial 80 W CO_2 laser engraver suitable for scalable production of elements for optical and optoelectronic applications. Two Ge concentrations (6 at% and 15 at%) were used to alter the dimensions of the Ge cap on the end of the fiber.

2. Experiment

The SiGe core material with a silica cladding were prepared by the molten core fiber drawing method [11] at a temperature of ~1950° C. Prior to loading, the inner surface of the silica cladding tube was coated with a thin interfacial layer of $Ca(OH)_2$ to reduce interactions between the silica cladding and the molten semiconductor [12]. Large diameter fiber, also known as cane, was used in this study, with cores of either 6 or 15 atomic percent (at%) Ge, the remainder being Si. The glass outer diameter was 2000μm with a core of 175μm for the 6 at% fibers, and the 15 at% fiber diameters were 800 μm(glass) and 75μm(core).

Laser processing of the resultant fiber was designed to test scalable production of arrays using a commercial 80W CO_2 laser engraver (4060, BRM Lasers) for fiber processing. The primary wavelength (10.6 μm) is absorbed by the silica cladding and melts the core via conductive heating, as in the work of Healy et al. [6]. As shown in Fig. 1(a), the end-face of the fiber was illuminated to create a vertical thermal gradient. A ZnSe cylindrical lens with 50mm focal length was used, and the fiber was place between 0–8 mm from the focal point at input powers from 22-30W. Intensity was estimated to be 800W/cm^2 at the focal point for a power setting of 25W. The

#377984 https://doi.org/10.1364/OME.9.004301
Journal © 2019 Received 16 Sep 2019; revised 8 Oct 2019; accepted 9 Oct 2019; published 14 Oct 2019

Optical Materials EXPRESS

annealing time was varied from 30 to 80 seconds. After a melt zone was established, the power level was decreased at a rate of ~ .07 W/s to aggregate Ge at the top of the fiber. While variations in composition and emissivity of the alloy prevented accurate calibration, the temperature profile was approximately linear with a gradient of ~4000K/cm and a maximum temperature at the irradiated end in excess of 1900 °C. For Ge cap formation the temperature gradient was key, as thermomigration is the primary mechanism. Details of the temperature profile are less critical than the slope.

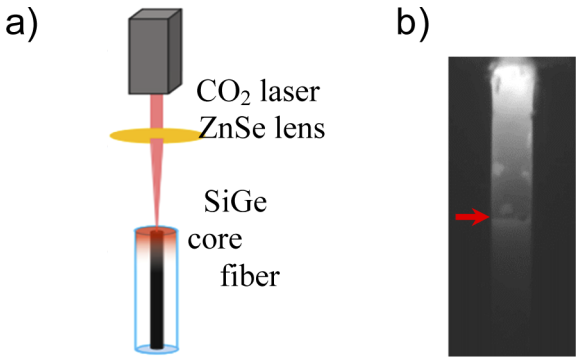

Fig. 1. a) Schematic of the laser end-annealing fiber set-up. b) USB camera image of end-annealing melt zone. Red arrow indicates solid-liquid boundary.

A conventional CMOS camera (Thorlabs DCC3240M) was used to collect visible emission from the heated fiber, which allowed imaging of the melt zone (Fig. 1(b)). Clear boundaries are observable due to the difference in the emissivity of the liquid and solid [8]. To acquire optical spectra, one Ge-cap sample (25W, 60s, average 0.07 W/s reduction) was prepared with the inhomogeneous region at the untreated end of the fiber removed, and one was prepared with both the inhomogeneous and Ge-rich regions removed. These were mounted to permit longitudinal illumination. A pure silicon core fiber, 12 mm long and annealed following the procedure of Healy, et al. [6] was used as a standard.

The transmission of the fibers was characterized with both monochromatic and broadband sources. Images of the spatial patterns of the transmitted light were made using a 10mW diode emitting at 1.55μm (Q-Photonics), either butt-coupled to the sample using a single mode fiber or end-illuminated with a lensed fiber (Oz Optics). A fiber coupler/splitter (ThorLabs) was used to combine the IR with the output of a visible diode used for alignment and to assure that no light was transmitted through the glass surrounding the semiconductor core. Images were acquired with an infinity corrected 20x microscope objective and a near IR camera (Edmund Scientific). A fiber-coupled white-light plasma source (Energetiq EQ-99x) was combined with an InGaAs spectrometer (BWTech) for characterization of the transmission over a wavelength range from 900-1400 nm.

Energy dispersive X-ray spectrometry (EDX) measurements were performed using a Hitachi TM3000 SEM, and X-ray tomography (XCT) was performed using an XT H 225 ST micro-CT system from Nikon Metrology NV, using a tungsten target, a source current of 47 μA and acceleration voltage of 145 kV. The samples were mounted with their long axis parallel to the vertical tomography axis and scanned in the range 0° to 360°.

Optical Materials EXPRESS

3. Results and discussion

3.1. SiGe fibers – 6 at% Ge

During CO_2 laser heating, thermomigration draws Ge-rich material through the Si, as reported by Coucheron, et al. [8], and Ge rich liquid accumulates in the highest temperature region. During cooling, Si solidifies first and preferentially, resulting in Ge-enrichment of the remaining liquid [8,13] and differing compositional profiles depending on the annealing geometry. For a fiber that is homogenized by constant velocity translation of the beam along the length of the sample, a dynamic equilibrium is established between the Ge available at the input end and what is deposited at the solidification front. This results in a fiber with a slight depletion at the start of the homogeneous scanned region, and an enrichment at the end [8]. For end-annealed fibers, the Ge-rich droplets recruited from the material near the distal end of the melt zone will accumulate at the illuminated surface as the power is reduced. This results in a cap with up to 100 at % Ge, similar to what is found when bulk SiGe is solidified at high rates [14]. EDX results for the Ge distribution as a function of laser power and anneal time for 6 at% Ge fibers are shown in Fig. 2. Of these variables, the laser power (and consequent length of the melt zone) affected the results most strongly, due to the recruitment of Ge from a greater depth. Longer heating times allowed a slight increase in the depth due to heat conduction, and larger fiber diameters reduced the cooling rate.

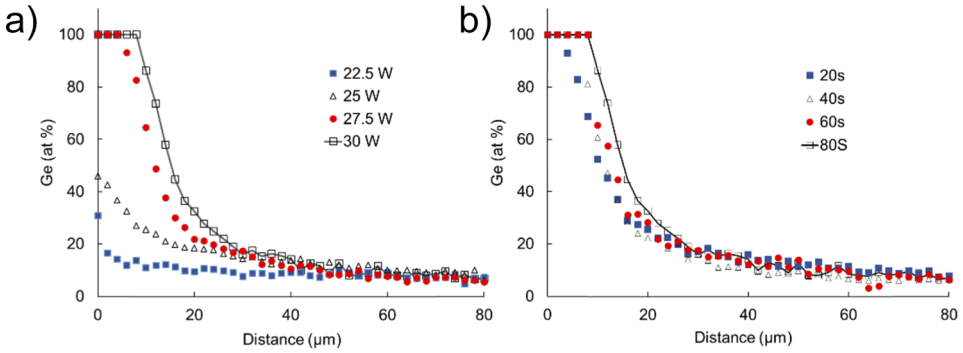

Fig. 2. Longitudinal variation in Ge concentration for end-annealed fibers (6 at% Ge, 75 μm core) as a function of a) power with 80s on focus, and b) anneal time (single step reduction), for an input power of 30 W on focus.

To make samples with the greatest segregation, stepwise power reduction was used as single step power reductions caused rapid recrystallization and constitutional supercooling. While cooling rate was not a major determinant of the final concentration value at the tip, gradual power reduction, to allow Ge diffusion away from the solidification boundary, resulted in the largest Ge-rich caps. Figure 3(a) shows XCT of a fiber cooled slowly (1W power reduction each 15s); Ge appears bright due to the higher atomic mass, and the horizontal lines that can be seen are due to the digital nature of the power control. The region below the bottom red arrow is the untreated, inhomogeneous fiber. Figure 3(b) shows the Ge concentration as a function of position with an inset that highlights the behavior in the regions of low Ge concentration.

3.2. SiGe fibers –15% Ge

To assess the optical properties of the fibers, both transmission spectra and infrared camera images were acquired for 15 at% Ge samples annealed at 25W for 60s; the higher percentage of Ge facilitated the aggregation of a larger enriched zone. The 100 at% Ge cap was 18-20 μm thick, dropping to a concentration of 12 at% at a depth of 80-100 μm with a profile similar to

Optical Materials EXPRESS

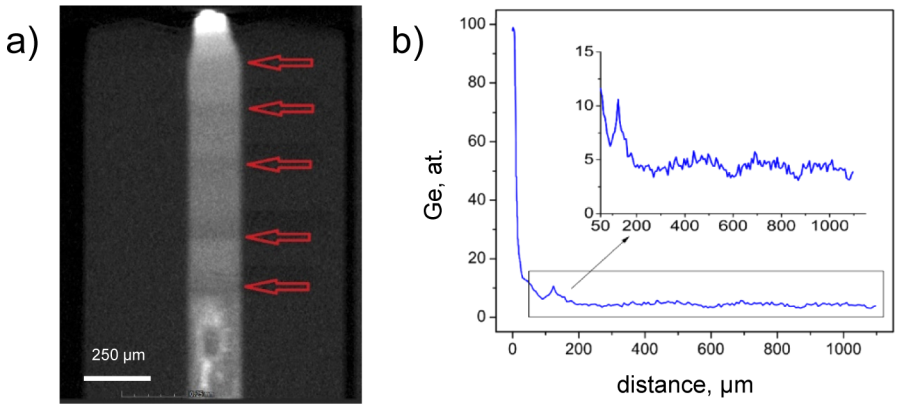

Fig. 3. a) an XCT image for a 6 at% end-annealed fiber, (25W for 80 s) and b) an EDX line scan of the Ge concentration. Stepwise reduction in power results in variations in Ge concentration (arrows).

as seen in Fig. 2(b). The transmission was measured longitudinally through a Ge-cap sample 825 μm long and one where the cap had been polished off ("cap removed"; 300 μm long). As the melt depth could not be increased arbitrarily, samples were prepared identically, and removal of the cap resulted in a shorter sample for the second measurement. In addition, a spectrum was acquired with the same source through a 12 mm long Si fiber. The spectra, as shown in Fig. 4(a), are normalized, and as such, primarily useful for comparing the absorption onsets for the different samples. For the end annealed fibers, the difference in the sample lengths for a constant absorption coefficient would be expected to lead to a factor of only two in measured transmission, so differences seen here are indicative of compositional changes, not scale. The Ge-cap sample shows absorption below 1300 nm. This is consistent with 40 at% Ge, and an energy gap of ~0.93 eV [15]. The 'cap removed' fiber had an average concentration of ~4% Ge, which, following Braunstein et al [15], would result in a change of the absorption edge of approximately 0.04 eV, or ~60 nm compared to pure silicon. Given the differences in the lengths of the samples and uncertainties in the coupling efficiency, the coincidence of the absorption edges of these two samples is within experimental error.

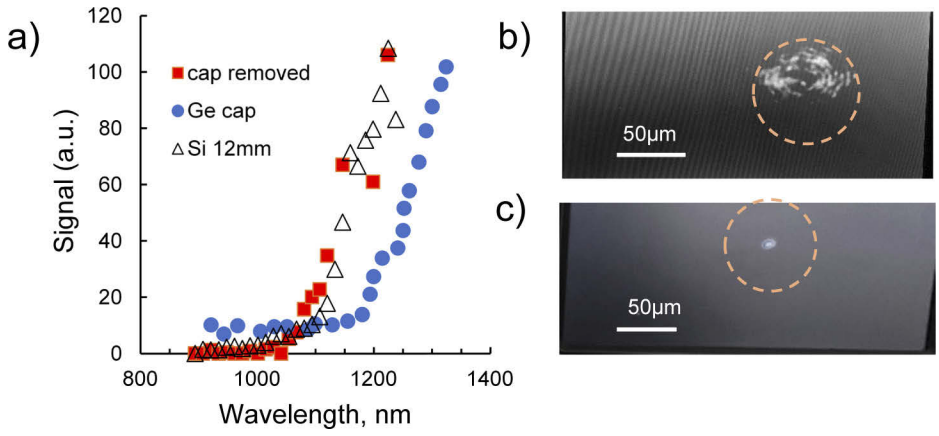

Fig. 4. a) Normalized transmission spectra through Ge cap, cap-removed and pure silicon fibers. b) Image of 1.55 μm transmission through a homogeneous core, and c) image through Ge-cap sample. The brown circles indicate the outer edges of the core.

Optical Materials EXPRESS

Figure 4(b) and 4(c) display the infrared (1.55 μm) images through the cap-removed and Ge-cap samples, showing that the curved tip collects and collimates the heavily multimode transmission through a radially homogeneous core. While the intensity/mode structure of a polycrystalline fiber varied as the input fiber was displaced across the polished input face of the core, the output spot of the Ge-cap fiber was stable when illuminated off-axis, indicating the lens-like structure was collecting and focusing the transmitted light. The homogeneous fiber was shorter, but the pattern observed is typical of translationally annealed fibers with lengths of several mm [16]. The minimum diode current needed for an image with the Ge cap fiber corresponded to an intensity ~15x smaller than that required for visualization of the maximum intensity regions through the shorter, cap-removed fiber. Differences in the indicated diameter of the core are due to changes in magnification of the optical system.

3.3. SiGe fiber array

To demonstrate the scalable possibilities of the process, a linear array of fibers with 175 μm cores and 6 at% Ge was assembled with a glass frit, and the laser was scanned across the top end of the fiber array. This process also leads to the concentration of Ge on the tips of the fibers, as shown in Fig. 5. With the process parameters chosen (30W, 0.1 mm/s), the depth of reduced Ge material was 655,642, and 618 μm measured from the top of each cap, due to imperfect vertical alignment and variations in thermal contact as evidenced by the confluence of the second and third fibers. The slight necking down of the core likely arises from competition between the surface tension of the glass and semiconductor. The glass cap was minimized, and reactive ion etching [17] could be used to remove the residual oxide if desired.

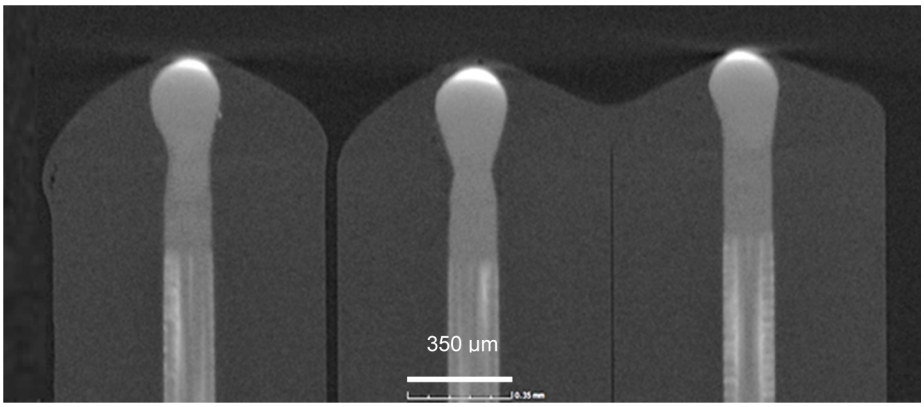

Fig. 5. XCT of end-annealed SiGe fiber array.

4. Conclusion

The ability to modify the local composition of SiGe core optical fibers after fabrication provides a route for scalable production of gradient structures such as those demonstrated here; these have potential application in devices such as solar cells [18] and detector arrays. While there have been significant advances in the production of in-fiber structures, the fabrication of devices with the potential for end-face electrical contacts is a major step forward. Bandgap modification is indicated by the shift in the transmission edge; this suggests the possibility of in-situ fabrication of photodiodes. Solar cells could be fabricated using an array of vertical Ge-cap pillars polished into a wafer, with tunnel junctions fabricated on the Ge rich side, following the design of Jang, et al [19]. Clear evidence of a lensing effect due to the curved end-caps is seen in transmission

Optical Materials EXPRESS

images, and this may be of use in fiber-based diagnostics and surgery requiring long-wavelength radiation.

Funding

Vetenskapsrådet (2016-04488); Norges Forskningsråd (262232); Knut och Alice Wallenbergs Stiftelse (2016.0104); J. E. Sirrine Foundation.

Disclosures

The authors declare no conflicts of interest.

References

1. R. He, T. D. Day, M. Krishnamurthi, J. R. Sparks, P. J. A. Sazio, V. Gopalan, and J. V. Badding, "Silicon p-i-n Junction Fibers," Adv. Mater. **25**(10), 1461–1467 (2013).
2. A. C. Peacock, P. Mehta, L. Shen, F. H. Suhailin, N. Vukovic, and N. Healy, *Silicon Fibre Devices for Nonlinear Applications* (IEEE, 2014).
3. A. C. Peacock and N. Healy, "Semiconductor optical fibres for infrared applications: A review," Semicond. Sci. Technol. **31**(10), 103004 (2016).
4. A. C. Peacock, J. Campling, A. F. J. Runge, H. Ren, L. Shen, O. Aktas, P. Horak, N. Healy, U. J. Gibson, and J. Ballato, "Wavelength Conversion and Supercontinuum Generation in Silicon Optical Fibers," IEEE J. Sel. Top. Quantum Electron. **24**(3), 1–9 (2018).
5. P. Mehta, N. Healy, T. D. Day, J. R. Sparks, P. J. A. Sazio, J. V. Badding, and A. C. Peacock, "All-optical modulation using two-photon absorption in silicon core optical fibers," Opt. Express **19**(20), 19078 (2011).
6. N. Healy, M. Fokine, Y. Franz, T. Hawkins, M. Jones, J. Ballato, A. C. Peacock, and U. J. Gibson, "CO_2 Laser-Induced Directional Recrystallization to Produce Single Crystal Silicon-Core Optical Fibers with Low Loss," Adv. Opt. Mater. **4**(7), 1004–1008 (2016).
7. F. H. Suhailin, L. Shen, N. Healy, L. Xiao, M. Jones, T. Hawkins, J. Ballato, U. Gibson, and A. C. Peacock, "Low Loss Tapered Polysilicon Core Fibers," in CLEO Paper SF2P.5 (OSA, 2016).
8. D. A. Coucheron, M. Fokine, N. Patil, D. W. Breiby, O. T. Buset, N. Healy, A. C. Peacock, T. Hawkins, M. Jones, J. Ballato, and U. J. Gibson, "Laser recrystallization and inscription of compositional microstructures in crystalline SiGe-core fibres," Nat. Commun. **7**(1), 13265 (2016).
9. A. Gumennik, E. C. Levy, B. Grena, C. Hou, M. Rein, A. F. Abouraddy, J. D. Joannopoulos, and Y. Fink, "Confined in-fiber solidification and structural control of silicon and silicon–germanium microparticles," Proc. Natl. Acad. Sci. U. S. A. **114**(28), 7240–7245 (2017).
10. A. Gumennik, L. Wei, G. Lestoquoy, A. M. Stolyarov, X. Jia, P. H. Rekemeyer, M. J. Smith, X. Liang, B. J.-B. Grena, S. G. Johnson, S. Gradečak, A. F. Abouraddy, J. D. Joannopoulos, and Y. Fink, "Silicon-in-silica spheres via axial thermal gradient in-fibre capillary instabilities," Nat. Commun. **4**(1), 2216 (2013).
11. J. Ballato and A. C. Peacock, "Perspective: Molten core optical fiber fabrication—A route to new materials and applications," APL Photonics **3**(12), 120903 (2018).
12. E. F. Nordstrand, A. N. Dibbs, A. J. Eraker, and U. J. Gibson, "Alkaline oxide interface modifiers for silicon fiber production," Opt. Mater. Express **3**(5), 651–657 (2013).
13. H. Y. S. Koh, Rapid Melt Growth of Silicon Germanium for Heterogeneous Integration on Silicon (PhD thesis, Stanford University, 2011).
14. N. Hussain, A. M. Mullis, and N. Haque, "Effect of cooling rate on the microstructure of rapidly solidified SiGe," Mater. Charact. **154**, 377–385 (2019).
15. R. Braunstein, A. Moore, and F. Herman, "Intrinsic Optical Absorption in Germanium-Silicon Alloys," Phys. Rev. **109**(3), 695–710 (1958).
16. T. Sørgård, K. Mühlberger, W. Wu, X. Yang, T. Hawkins, J. Ballato, F. Laurell, M. Fokine, U. J. Gibson, and U. J. Gibson, "Reduced loss in SiGe-core optical fibers," in CLEO, Paper SF3I.6 (OSA, 2018)
17. L. M. Ephrath, "Selective Etching of Silicon Dioxide Using Reactive Ion Etching with CF_4-H_2," J. Electrochem. Soc. **126**(8), 1419–1421 (1979).
18. F. A. Martinsen, B. K. Smeltzer, M. Nord, T. Hawkins, J. Ballato, and U. J. Gibson, "Silicon-core glass fibres as microwire radial-junction solar cells," Sci. Rep. **4**(1), 6283 (2015).
19. J. Jang, J. H. Song, H. Choi, S. J. Baik, and S. Jeong, "Photovoltaic light absorber with spatial energy band gradient using PbS quantum dot layers," Sol. Energy Mater. Sol. Cells **141**, 270–274 (2015).